Interactive comment on "New image measurements of the gravity wave propagation characteristics from a low latitude Indian station"

Anonymous Referee #2

The manuscript presents some new observations of mesospheric gravity waves using an all-sky imager located in Southern India. As mentioned in the text, numerous similar observations have been done in the past 30 years. Though measurements from this part of the world are scare, this data set doesn't bring anything really new. Furthermore, the amount of data is very small since it encompasses only a 2-month period during 3 years, due to limited sky conditions. This manuscript appears more like an observation report than a full scientific paper. The analysis technique is also rudimentary. I would suggest to the authors to read papers like Garcia et al., 1997, Cobble et al., 1998, or Tang et al., 2002; 2005 for improved analysis methods.

Response: Our sincere thanks to the reviewer. We are still developing the analysis methods and surely, in future we will come up with better image analysis method. We hope reviewer will agree that in order to get the wave characteristics, such as the wavelength and phase speed, the method used provides correct information.

I don't think this work should be published as it is. Nevertheless, the complete data set might be of some interest after a full investigation. Both mesospheric emissions (OH and OI) observed with the all-sky imager should be analyzed. Even with poor sky conditions, the other months should also be processed.

Response: As we mentioned in the introduction section, getting cloud free night over our location is very rare. To a dismay to us, since the installation of imager, we could get good data only during March – April months. We hope that reviewer will understand our view in reporting only March and April months.
Further, the imager was optimized to view OI 557.7 nm as well as OI 630 nm emissions together with OH (846 nm). In doing this, the OH images are not well focused and unless there is a very strong gravity wave event, we can not estimate the wavelength properly. Therefore, we have used only OI557.7 nm data.
Page: 4; line:8-9;

The possible correlation between convective regions and GW propagation could then be confirmed or not.

Response: Now, we have done reverse ray tracing also. And the results are discussed in the present form of the manuscript.

Minor comments:

I don't understand why you crop the images to 90deg if you also unwrap them to correct for lens distortion. This rather small field of view probably affects the range of horizontal wavelengths you can measure. You also need to provide errors on your measurements.

Response: The imager is placed inside a concrete housing where opening is made such that it avoids the background illumination. In order to remove the laboratory walls we have cropped the images. Further, to remove the lens curvature effect we have done

unwrapping. This however, does not introduce any error as the error is a function of pixel size on which the image is focused, which is 0.8 km. We have mentioned it at page 4; line: 14-16.

P.2: l. 6: events, the grammar should be improved as well

Response: We have attempted to correct it in all our capacity.

l. 9: occurrence instead of occasions

Response: changed. Page: 1; line: 16

l. 10: was a possible source for the...

Response: modified. Page: 1; line: 18

l. 13-15: not clear

Response: modification has been done. Page: 1; line: 24-25

l. 20-21: "to observe the GW signatures" or "to measure the GW parameters"

Response: modified. Page: 1; line: 28

l. 21: The primary advantage of the imaging technique...

Response: modified. Page: 2; line: 4

l. 22: remove "altitude"

Response: removed.

p.3: l. 3: For about a decade... (it's more about 3 decades!)

Response: sentence has been corrected. Page: 2; line: 12

l. 15: during summer

Response: modified. Page: 3; line: 15-18

l. 29: the said period

Response: sentence has been modified. Page: 3; line: 16-22

p.4: l. 6: remove "clear sky"

Response: removed.

l. 7: a field of view (FOV) of 180...

Response: correction has been made. Page: 3; line: 27-28

l. 11-12: "Yoda English"

Response: modification has been done. Page: 4; line: 2-5

l. 15: during the operations.

Response: modified.

l. 16: we bin the images to 2x2 pixels...

Response: correction has been done. Page: 4; line: 4

l. 19: current exposure times are as follow: 15s...

Response: correction has been made. Page: 4; line: 7

21: Further details about the NAI are given in Taori et al., 2013

Response: modification has been done. Page: 4; line: 10

l. 26: unwarped

Response: corrected. Page: 4; line: 13

p.5: l. 1: we used a median filter.

Response: correction has been made. Page: 4; line: 17

l. 10: to enhance the wave fronts

Response: correction has been made. Page: 4; line: 16

p.6: l. 10: a phase velocity

Response: correction has been made. Page: 4; line: 33

p.7: l. 6: Most of...

Response: correction has been done. Page: 7; line: 21

l. 20: (b) average of the daily mean...

Response: correction has been made. Page: 8; line: 7

l. 21: Remove last sentence

Response: removed.

l. 25: missing something! maybe "propagation angle in the month of April"?

Response: Sentence is reformulated. Page: 8; line: 8-22

l. 28: "propagating towards Northwest" or "propagating northwestward"

Response: modification has been done. Page: 8; line: 16-17

p.8: l. 3-4: southeast part of the map

Response: modification has been done. Page: 8; line: 23

p.9: l.4: very remote possibility

Response: We have discussed this at page 10; line 10-14.

Mesospheric gravity wave characteristics and identification of their sources near to the spring equinoxial months over Indian low latitudes

M. Sivakandan[1], I. Paulino[2], A. Taori[1], and K. Niranjan[3]

[1]{National Atmospheric Research Laboratory (NARL), Gadanki, 517112, India}

[2]{Universidade Federal de Campina Grande (UFCG), Campina Grande, Brazil}

[3]{Department of Physics, Andhra University, Visakhapatnam, 530003, India }

Correspondence to: A.Taori (alok.taori@gmail.com)

Abstract

We report OI557.7 nm night airglow observation with the help of a CCD based all-sky camera from a low latitude station, Gadanki (13.5^{o}N; 79.2^{o}E). Based on the data collected during March and April over three year, from 2012 to 2014 (except March 2013), we characterize the small scale gravity wave properties. During this, 50 strong gravity wave events and 19 ripple events were detected. The horizontal wavelengths of the gravity waves are found to vary from 12 km to 42 km with the phase velocity ranging from **20 to 90 m/s**. In most cases, these waves were propagating towards north with only a few **occurrence** of southward propagation. **The outgoing long wave radiation (OLR) suggested that tropospheric convection was a possible source for generation of the observed waves. In the present novel investigation from Indian sector, each of the wave event were reverse ray-tracked to their sources. It was found that approximately 66% of the events were triggered directly by the convection.**

Introduction

The variability in the middle atmospheric parameters is often attributed due to the energy and momentum deposition by gravity waves [e.g., *Fritts and Alexander,* 2003]. There are many techniques to study the gravity wave activities in the middle and upper atmosphere, such as radio, optical and insitu as well as space borne. In order to observe the gravity wave parameters in the atmosphere, radars, lidars, photometers, rockets and satellite instruments have been used [e.g.,*Smith*, 2012]. However, **small scale gravity waves remain the least understood due to the instrumental limitation which can provide**

the scale sizes, propagation direction together with its temporal evolution characteristics. In this regard, ground based airglow imaging is an important tool to estimate the gravity wave signatures. The primary advantage of the imaging is that it provides a 2 - dimensional view at the chosen airglow emission and thus it has the capability to determine the horizontal scales and propagation direction of the gravity waves. Further, at a given place it provides the temporal evolution of the gravity wave induced oscillations. As the field of view of imagers at mesospheric altitudes may cover a horizontal distance of **300 – 350 km**, such measurements are highly suited for the waves having small scales (horizontal wavelength < 150 km), short periods (periods < 1 hour) and long enough vertical wavelengths (>10 km**) [*Liu and Swenson*, 2003]**.

Since **about last three** decades, capabilities of airglow imaging have been widely utilized to analyze the gravity wave characteristics [e.g., *Taylor and Hapgood*, 1988; *Nakamura et al.*, 1999; *Walterscheid et al.*, 1999; *Medeiros et al.*, 2003; *Ejiri et al.*, 2003; *Kim et al.*, 2010; *Li et al.*, 2011a,b]. Particularly, *Nakamura et al.*, [1999] utilized 18 months of OH imager observations at Shigaraki (34.9◦ N, 136.1◦ E) and reported that the gravity waves propagated eastward (westward) in the summer (winter) with horizontal wavelength varying from 10 km to 45 km. *Medeiros et al.*, [2003] analyzed 12 months observation at Cachoeira Paulista (23◦ S, 45◦ W) and found that gravity waves exhibited preferential propagation directions, with southeast propagation in the summer and northwest in the winter with wavelength range 5-60 km. Using 1 year OH Meinel and OI (557.7 nm) band image data at Rikubetsu (43.5◦ N, 143.8◦ E) and Shigaraki (34.9◦ N, 136.1◦ E) in Japan from October 1998 to October 1999, *Ejiri et al.*, [2003] reported that gravity waves propagated mostly to the north or northeast during in summer at both sites with wavelengths in the range 10-58 km. However, gravity waves propagated to the west at Rikubetsu and to the southwest at Shigaraki in winter. In a more recent report, *Kim et al.*, [2010] used OH, O_2 and OI557.7nm data from Mt. Bohyun, Korea (36.2◦ N, 128.9◦ E) and found that gravity waves propagate westward during fall and winter and eastward during spring and summer. The wavelengths were found to be in 10-45 km range.

From Indian sector, there are few reports [*e.g.Mukherjee 2003, Mukherjee et al 2010, Pragati et al 2010, Lakshmi Narayanan and Gurubaran, 2013., Parihar and Taori 2015*] which documents the small scale gravity waves characteristics. For example, using five months of OH airglow imager data during January to May, 2008, at Allahabad (25.45◦N, 81.85◦E), *Pragati et al [2010]* reported that most of the small scale

gravity waves propagates towrads North and North-East direction in March and May. Further, using the same data set *Mukherjee et al [2010]* studied the wind filtering effect of the gravity waves. Likewise, using one year of airglow imager data during 2007 *Lakshmi Narayanan and Gurubaran, [2013]* reported the seasonal variation of the gravity waves characteristics over Tirunelveli (8.71^o N, 77.81^o E). Recently, *Parihar and Taori [2015]* investigated the long distance propagating gravity waves using the coordinated bi-station airglow data (Airglow photometer over Gadanki (13.5^o N, 79.2^o E), and all sky airglow imager over Allahabad (25.5^o N, 81.9^o E). They concluded that convection might be a source of the noted long distance gravity wave events. However, none of these reports addressed the exact sources of the waves.

It is important to note that being a tropical location, the availability of optically clear sky makes the statistics biased. Therefore, in the present report we have taken the data in March-April 2012 and 2014 and April 2013, when the maximum number of cloud free nights are monitored [e.g., *Taori et al.*, 2012] over Gadanki (13.5^o N; 79.2^o E). First time in indian sector, we show the gravity wave charactistics together with the reverse ray-traced sources of these waves. We use outgoing Long wave radiation (OLR) obtained from the National Oceanic and Atmospheric Administration (NOAA) and a reverse ray tracing analysis for the above purpose.

Instrumentation and data analysis

The all sky airglow imager of the National Atmosphere Research Laboratory (NARL) has been installed in March 2012 at Gadanki (13.5^o N, 79.2^o E) in March 2012. Since then, this NARL Airglow Imager (NAI) has carried out regular night airglow observations during moonless, cloudless nights. The front optics of NAI uses a fish eye lens **having a field of view (FOV) 180^o** (**current FOV is limited to 117^o due to NAI housing to avoid the background illumination at low elevation and to avoid nonlinearity of the pixels at higher zenith angles**). Its filter chamber contains three different interference filters, namely 840 nm for OH emission (peak altitude ~87 km), OI557.7nm emission (peak altitude ~97 km) and **OI630 nm** emission (peak altitude ~250 km). In order to maintain the constant temperature a thermo-electric temperature controller is attached to the filter chamber. **A camera lens focuses the light on the PIXIS-1024B CCD sensor, which is thermoelectrically cooled**. **In the present set-up, we bin the images to 2 x 2 pixels making an effective 512x512 super pixel image on the chip to enhance the signal-to-**

noise ratio. Depending on the compromise **between** the background luminosity, interference filter transmission and actual airglow brightness, at **current** exposure time are **15s for OH and 110s for both, OI557.7nm and OI630 nm emission monitoring. The imager was optimized to view OI557.7 nm as well as OI630 nm emissions together with OH (840 nm). Further details about** the NAI are given in *Taori et al.*,[2013].

In this present study, using earlier mentioned dataset, we could get 32 clear sky night data. From raw images we have cropped the images for 117^o full field of view to remove the background walls of our laboratory from the images. Further, we **unwarped** the images for **barrel** distortions to linearize the scales. **This however, does not introduce any significant difference in the wavelength estimation as the error is a function of pixel size on which the image is focused, which in the present case is ~0.8 km.** At last **we enhance the wave fronts** by contrast adjustment (for better visibility). In order to remove the stars we **used a** median filters. In thus obtained, processed images, continuous bright and dark band which **persist** in more than three consecutive images are considered as the structure depicting a wave event**.** This analysis is performed on all the data. We note that in 32 days of data**, 69 wave events were prominent**. **Among these, 19 events** did not show any phase propagation and were moving with its background. Those wave events are considered as ripples (which may be arising due to Kelvin Helmholtz instability occurring due to the wave dissipation) and thus have not been considered as propagating gravity waves. An example of a gravity wave event is shown in **figure 1.** In this figure, **green color box emphasize the presence of consecutive bright and dark bands.** The propagation is identified by cross correlating the position of these fronts from one image to another in consecutive images. Further, the estimate of propagation angle is done by measuring the angle between the yellow line (shown as a yellow line with an arrow indicating the direction of propagation) with the horizontal line parallel to **the north** direction. In order to get the horizontal wavelength of the observed wave event, we took the perpendicular pixels of wave phase (yellow colored arrows) and plot the gray count values. The distance between two peaks provides the horizontal wavelength estimates (in this particular wave event horizontal wavelength is estimated to be ~14 km). To calculate **a** phase velocity (Vp=displacement/time-difference) of the wave event, first we calculate the phase displacement of the wave from one image to the other (for example, if the position of a wave phase is (x_1, y_1) in the first image and in the second image the position is (x_2, y_2), then the displacement is defined as, $d = \sqrt{(x_2 - x_1)^2 + (y_2 - y_1)^2}$). In the case shown, the observed phase velocity is ~23 m/s, the angle of wave propagation is ~55^o.

We performed this analysis on the full data set (i.e., 50 wave events of which 21 events in the year 2012, 5 events in the year 2013 and 24 events in the year 2014) and wave characteristics obtained as explained above are presented in this report.

2.1 Ray tracing method:

According to the formalism of *Lighthill [1978]*, if a gravity wave packet is propagating in a fluid with the background wind $\vec{V}(\vec{x}) = (u, v, w)$, then its evolution can be described by:

$$\frac{dx_i}{dt} = V_i + \frac{\partial \omega_{Ir}}{\partial k_i} = V_i + c_{gi} \quad \text{..... (1)}$$

and

$$\frac{dk_i}{dt} = -k_j \frac{\partial V_j}{\partial x_i} - \frac{\partial \omega_{Ir}}{\partial x_i} \quad \text{..... (2)}$$

where $\omega_{Ir} = \omega_{Or} - \vec{k}.\vec{V}$ is the intrinsic frequency of the gravity waves, ω_{Or} is the observed frequency, $\vec{k}$ is the wave vector, $\vec{x}$ is the position of the wave in a given time, c_{gi} is the group velocity, $i, j = 1, 2, 3$ and repeated indices imply a summation. It means that the temporal evolution of a gravity wave in the atmosphere can be followed if its position and wave vector are known, in a given time, However, the knowledge of background wind and temperature are necessary as well.

In the present work, all of 50 observed gravity waves were reversed ray traced, in order to investigate the likely sources of them in the troposphere. The initial position of the gravity waves has been assumed to be equal to the geographic coordination of the observatory and the altitude of the OI557.7nm airglow layer peak, i.e., $\vec{x}(t = 0) = (x, y, z) = (79.2^o\text{E}, 13.5^o\text{N}, 97\ \text{km})$. The initial wave vector was taken from the OI557.7nm images and from the dispersion relation, that is, $\vec{k}(t = 0) = (k, l, m) = \left(\frac{2\pi}{\lambda_x}, \frac{2\pi}{\lambda_y}, m\right)$, where $\lambda_H^2 = \lambda_x^2 + \lambda_y^2$ is the horizontal wavelength. The vertical wave number at the OI557.7nm layer was obtained using the *Marks and Eckermann [1995*] dispersion relation, which excludes acoustic waves, i.e.,

$$m^2 = \frac{(k^2+l^2)N^2}{\omega_{Ir}^2} - (k^2 + l^2) - \frac{1}{4H^2} \quad \text{..... (3)}$$

where N^2 is the buoyancy frequency and H is the scale height.

The background wind used as the input to the ray tracing model was based on the Horizontal Wind Model *[HWM-07; Drob et al., 2008]* and the temperature profiles were obtained from Naval Research Laboratory Mass Spectrometer and Incoherent Scatter Radar model *[NRLMSISE-00; Picone et al., 2002].* In addition, comparison between the ray paths for the gravity waves using the HWM model and no wind conditions were made in order to evaluate the effects of the wind in the propagation of the gravity waves. Further description about this ray tracing model can be found in [*Vadas and Fritts 2005,2009 and Paulino et al., 2012]*.

Results and Discussion

First, we present the composite results for the years 2012-2014 to show the overview of the results. We note that horizontal wavelengths of the observed wave events are found to vary from 10 km to **42 km** (**figure 2**). Among this distribution, about half of the wave events **have** their horizontal wavelengths in 10-25 km range and 22% wave events were noted in 30-35 km wavelength range. It is evident from **figure 2** that more than 90% wave events are **have** their wavelength less than 35 km. The estimated horizontal phase velocity distribution of the observed wave events is shown in **figure 3**. Phase velocity of the noted wave events are vary from 20 m/s to 90 m/s. From this ~78% of the wave events show the phase velocity less than 50 m/s. Using the observed horizontal wavelength and phase speed we have calculated the **phase period** of the observed wave events which is shown in **figure 4**. The periods of observed gravity waves are found to be in 4 min to 20 min range. And about 90% waves have their periods in 6 min to 15 min range with only 1% of waves having their periods more than 15 min.

Wave propagation and sources of the wave:

In Figure 5(a) (polar plot) shows the horozontal propagation direction of the small scale gravity waves (left panel) and Figures 5b, c (right side) show the reverse ray paths [with zero wind condition (Fig 5b) and with estimated HWM model winds (fig 5c)] and their termination points. In the polar plot, red colored arrows indicate the wave propagation angle in March 2012 and 2014 and blue color arrows indicate the wave propagation angle in April 2012, 2013 and 2014. The dotted circles denote the horizontal phase velocity of the observed wave events with an interval of 20 m/s. Similarly, in right side plots red line(dot) indicates ray path(termination point) in March and blue line(dot) indicates ray path(termination point) in April. Most of the time waves propagate towards north with

only few events showing southward propagation (details of the wave propagation in different directions are given in **table 1**). An earlier report from Indian subcontinent by [*Lakshmi Narayanan and Gurubaran*, 2013] from Tirunelveli (8.7^{o} N), based on data corresponding to the year 2007 suggested that during equinox season waves mainly propagate towards the north**, presnet study also shows similar result**. As the waves propagate away from their source regions [e.g., *Pautet et al.*, 2005], it is prudent to suggest that the wave generations must be located somewhere in the south of the measurement location. In oder to identify the exact source mechanims we use reverse ray tracing technique that results are shown in righ side of the figure 5(b,c). Then we have compare the dermination points with NOAA daily mean OLR data. (the results are discussed in next paragaph).

A comparison of our results with some of the earlier small scale wave measurements is made in table 2 (please note that the list is not exhaustive). It is to note that, the wavelengths, phase velocity and observed wave periods are within the range reported by the earlier investigations. Further, as most small scale waves observed in mesosphere have their origin in lower atmospheric processes such as tropospheric convection, wind shear, wave-wave interaction or secondary wave generation [e.g., *Alexander*, 1996; *Holton and Alexander*, 1999; *Pandya and Alexander*, 1999; *Piani et al.*, 2000; *Fritts and Alexander*, 2003; *Taori et al.*, 2012; *Pramitha et al.*, 2015]. Numerous modelling as well as experimental evidences over equatorial latitudes suggest that most small scale waves with periods less than an hour have their sources in convective processes [e.g., *Horinouchi et al.*, 2003; *Nakamura*, 2003; *Pautet et al.*, 2005]. Of the particular relevance to our observations is the report by *Pautet et al.*, [2005], **based on** the 19 wave events it was clearly shown that waves were generated by the convection and propagated away from their sources (convective clouds). We investigate whether convection and associated processes are the prime potential sources for the perturbations noted in the middle atmosphere and ultimately were reflected in the upper mesospheric altitudes. For this, we carry out reverse ray tracing analysis (as mention earlier) and subsequently the termination points were compared with the daily mean NOAA-OLR**. The present investigation shows about ~66% wave events the soruces were located within the convective clouds and for another ~14% of wave events, source were located nearby the convective region. Remaining 20% wave events were generated purely by the non convective sources**. Further, to understand the monthly and yearly variation of the source region, we look into **average of the daily mean** NOAA-OLR for the days when airglow observations were made.

Figure 6a left side (polar polt) shows the propagation direction and phase velocity of the wave events noted in March-April 2012 and right side plots show the reverse ray tracing paths with their termination points (top panel show ray paths for zero wind condition-Figure 6(b) while the bottom panel show ray paths using HWM model wind Figure 6(c)). Similar to the figure 5 left side (polar plot), red colored arrows indicate the wave propagation angle in March and the blue color arrows indicate the wave propagation angle in April. Likewise, in right side plots red line (dot) indicates ray path (termination point) in March and bule line (dot) indicates ray path (termination point) in April. Further, out of 21 wave events 14 wave events are propagating towards north-west. Few waves were travelling towards the north-east while only 2 wave events having their propagation towards south. Ray path also shows the similar result but in opposite direction. The average of daily mean OLR data during the observations is plotted in Figure 7. In the OLR low intensity (<200) belongs to the deep convection. The left map shows the averaged OLR values for March month while the right map is for April 2012. The location of measurement is shown as asterick. It is clear that during the March month there is a deep convection occurring at the **southeast part of the map** hence the waves propagating away from these sources shall have the propagation in the north-west direction which is consistent with the observations. It is interesting to note that during April month apart from the deep convection at the southeast location, there is a convective patch on the southwest **side of the map**. In this regard, observations suggesting that in the April month waves propagated in the north-east and northwest directions (in figure 6a) are consistent with the fact that their sources were associated with the convective plumes noted in the OLR data. There are two wave events which show southward propagation (on 27 March 2012) which we showcase as special case in the following.

On 27 March 2012, we noted four wave events, two of them propagating towards north-west and another two waves progressing to the south-east (as mentioned earlier). On this night, the daily mean OLR data and reverse ray paths are plotted in figure 8. There was some convective process occurring in the north-west locations as well as a strong convection in south-east location. Together with the OLR patches, the ray path also terminates nearby the convective locations. There were some isolated convective process at 20^{o}N,76^{o}E (source, http://www.mosdac.gov.in) which may have triggered these waves. We reemphasis that only those events which could overcome the wind filtering mechanisms could be observed. Typical zonal and meridional winds during March-April

months over Tirunelveli (8.7^{o} N,77.8^{o} E) are reported to be ~15 m/s and 18 m/s [*Sivakandan et al.*, 2015] in 85- 100 km altitude range, and also that Horizontal Wind Model (HWM-07) wind estimates also suggest the maximum winds to be less than 20 m/s at these altitudes. Thus, waves having their phase velocity more than 20 m/s will not be blocked by the horizontal winds and may propagate to their preferred directions governed by the source properties. We believe that this is the reason we noted the waves have their phase velocity more than 20 m/s. Taking the above into the account, we believe that this event of abnormal wave propagation has been well captured by the reverse ray tracing analysis.

As mentioned earlier, the NAI could not be operated during March 2013 however, the propagation and phase velocity of the wave events noted in April **2013 as well as their reverse ray path results were plotted in Figure 9.** Out of 5 wave events, 3 waves were propagating to the northeast directions, 1 was propagating northwestward while 1 wave was propagating to the **southeast and the ray paths were derminates opposite to the wave propagation direction. Further, important think is that all** the waves had their phase velocity higher than 20 m/s. **The OLR data** corresponding to April 2013 events are plotted in **figure 10** where it is clear that there were convective regions in the southern side of the measuring site which most possibly triggered the waves which were propagating to the northeast and northwest directions with one of the event propagating to southeast direction, on this day **daily mean OLR shows convective region at around 20^{0} N lat; 70^{0}E lon (figure not shown here). Furtther, as in earlier cases, for all these wave events ray path also terminates to the convective region**.

The left side (polar plot) plot depicting the gravity wave propagation direction and phase velocity and right side plot depicting the reverse ray tracing results corresponding March-April 2014 is shown in **figure 11a,b,and c**. This year wave directions show deviations compared to the year 2014. In year 2012 waves propagated dominantly to the northwest while in 2014 waves are moving towards northeast with a substantial number of waves in southward directions. Similarly, ray paths terminate opposite direction of the wave propagtion shown in figure11 b,c. The OLR corresponding to the March and April 2014 are shown in **figure 12**. It is to **note** that there are convective processes occurring in southward as well as northward directions and thus the waves triggered by these sources are reflected in our measurements. Our ray racing results also conforming this. However, from the ray tracing termination point it is clear that, the waves propagating almost in zonal directions are not generated by the **convective origin. Of this, one of the event was discussed earlier to**

be caused by the wind shears [*Pramitha et al.*, 2015]. Other sources may be mesospheric-thermospheric body forcing, secondary waves [*e.g., Fritts and Alexander, 2003; Vadas and Fritts, 2009; Vadas and Liu, 2011*], where convection may ramain as a prime source (~66%) of gravity waves.

Summary

The image measurements of OI557.7nm nightglow during the spring season over Indian low latitudes show conspicuous signatures of upper mesospheric waves. The horizontal wavelengths ranged from 10 km to **42 km** and were mostly found to propagate towards the north side of the location of the measurements. Over the Indian subcontinent, often the lower atmospheric convection activities occur at the southern side of the location which we have also noted in the OLR data. The directions of wave propagation **and reverse ray tracing results were found to be consistent with the source being in the south, which suggest that ~66% observed wave events were purely generated by tropospheric convection and another 14% wave were coming from nearby the convective region. And remaining 20% waves were generated by purely non convective source mechanisms. Present investigation prominently shows that, convection and their associated process are the main source for the generation of small scale gravity wave over the low latitude Indian sector.**

Acknowledgements

The present work is supported by the Department of Space, Government of India. We acknowledge the help of Mr. Liyakat Basha, V. Kamalakar and R. Goenka for their help in carrying out night airglow measurements. We thank Ms. C. A. Smith of NOAA Earth System Research Laboratory for providing the interpolated OLR data (Source: www.esrl.noaa.gov/psd/data/gridded/data.interp_OLR.html). I. Paulino thanks to the CNPq for the financial support (grant no. 478117/2013-2)

References

Alexander, **M.** J., A Simulated Spectrum of Convectively Generated Gravity Waves: Propagation from the Tropopause to the Mesopause and Effects on the Middle Atmosphere, *J. Geophys. Res.*, *101*, 1571–1588, doi:10.1029/95JD02046, 1996.

Ding, F., H. Yuan, W. Wan, I. M. Reid, and J. M. Woithe, Occurrence characteristics of medium-scale gravity waves observed in OH and OI nightglow over Adelaide (34.5^0S, 138.5^0E), *J. Geophys. Res. D Atmos.*, *109*(14), 1–10, doi:10.1029/2003JD004096, 2004.

Drob, D.P., Emmert, J.T., Crowley, G., Picone, J.M., Shepherd, G.G., Skinner, W., Hays,

P., Niciejewski, R.J., Larsen, M., She, C.Y., Meriwether, J.W., Hernandez, G., Jarvis, M.J., Sipler, D.P., Tepley, C.A., O'Brien, M.S., Bowman, J.R., Wu, Q., Murayama, Y., Kawamura, S., Reid, I.M., Vincent, R.A., An empirical model of the Earth's horizontal wind fields: HWM07. *J. Geophys. Res.*, 113, 12304. doi:10.1029/2008JA013668, 2008.

Ejiri, M. **K., K. Shiokawa, T. Ogawa, K. Igarashi, T. Nakamura, and T. Tsuda,** Statistical study of short-period gravity waves in OH and OI nightglow images at two separated sites, *J. Geophys. Res.*, 108(D21), 4679, doi:10.1029/2002JD002795, 2003.

Fritts, D. C., and M. J. Alexander, Gravity wave dynamics and effects in the middle atmosphere, *Rev. Geophys.*, *41*(1), 1003, doi:10.1029/2001RG000106,2003.

Holton, J. R., and M. J. Alexander, Gravity waves in the mesosphere generated by tropospheric convection, *Tellus, Ser. B Chem. Phys. Meteorol.*, *51*(1 SPEC. ISS.), 45–58, doi:10.3402/tellusa.v51i1.12305, 1999.

Horinouchi, T, S. Pawson, K. Shibata, U. Langematz, E. Manzini, M. A. Giorgetta, F. Sassi, R. J. Wilson, K. Hamilton, J**. de Grandpre´,** and A. A. Scaife, Tropical Cumulus Convection and Upward-Propagating Waves in Middle-Atmospheric GCMs, *J. Atmos. Sci.*, *60*(22), 2765–2782, doi:10.1175/1520-0469(2003)060<2765:TCCAUW>2.0.CO;2, 2003.

Kim, Y. H., C. Lee, J. -K. Chung, J. -H. Kim, and H. -Y. Chun, Seasonal variations of mesospheric gravity waves observed with an airglow all-sky camera at mt. Bohyun, korea (36° N), *J. Astron. Sp. Sci.*, *27*(3), 181–188, doi:10.5140/JASS.2010.27.3.181, 2010.

Lakshmi Narayanan, V., and S. Gurubaran, Statistical characteristics of high frequency gravity waves observed by OH airglow imaging from Tirunelveli (8.7^oN), *J. Atmos. Solar-Terrestrial Phys.*, *92*, 43–50, doi:10.1016/j.jastp.2012.09.002, 2013.

Li, Q., J. Xu, J. Yue, W. Yuan, and X. Liu, Statistical characteristics of gravity wave activities observed by an OH airglow imager at Xinglong, in northern China, *Ann. Geophys.*, *29*(8), 1401–1410, doi:10.5194/angeo-29-1401-2011a.

Li, Z., Liu, A. Z., Lu, X., Swenson, G. R. and Franke, S. J.: Gravity wave characteristics from OH airglow imager over Maui, *J. Geophys. Res. Atmos.*, 116(22), doi:10.1029/2011JD015870, 2011b.

Lighthill, J., Waves in Fluids. *Cambridge University Press, New York*, 1978.

Liu, A. Z., and G. R. Swenson, **A modeling study of O_2** and OH airglow perturbations induced by atmospheric gravity waves, *J. Geophys. Res.*, 108(D4), 4151, doi:10.1029/2002JD002474, 2003.

Makela, J. J., and Y. Otsuka, Overview of nighttime ionospheric instabilities at low- and mid-latitudes: Coupling aspects resulting in structuring at the mesoscale, *Space Sci. Rev.*, *168*(1-4), 419–440, 2012.

Marks, C.J., Eckermann, S.D., A three-dimensional nonhydrostatic ray-tracing model for gravity waves: formulation and preliminary results for the middle atmosphere. *J. Atmos. Sci.*, 52, 1959–1984, 1995.

Medeiros, A. F., M. J. Taylor, H. Takahashi, P. P. Batista, and D. Gobbi, An investigation of gravity wave activity in the low-latitude upper mesosphere: Propagation direction and wind filtering, *J. Geophys. Res*., 108(D14), 4411, doi:10.1029/2002JD002593, 2003.

Medeiros, A. F., Takahashi, H., Buriti, R. A., Fechine, J., Wrasse, C. M. and Gobbi, D., MLT gravity wave climatology in the South America equatorial region observed by airglow imager, *Ann. Geophys*., 25(2), 399–406, doi:10.5194/angeo-25-399-2007, 2007.

Mukherjee, G.K., The signature of short-period gravity waves imaged in the OI 557.7 nm and near infrared OH nightglow emissions over Panhala, *J. Atmos. Solar-Terr. Phys.* 65, 1329-1335, 2003.

Mukherjee, G.K., Pragati Sikha, R., Parihar, N., Ghodpage, R., and Patil, P.T., Studies of the wind filtering effect of gravity waves observed at Allahabad (25.45_N,81.85_E) in India, *Earth Planets Space* 62, 309-318, 2010.

Matsuda, T. S., Nakamura, T., Ejiri, M. K., Tsutsumi, M. and Shiokawa, K.: New statistical analysis of the horizontal phase velocity distribution of gravity waves observed by airglow imaging, *J. Geophys. Res. Atmos.*, 119(16), 9707–9718, doi:10.1002/2014JD021543, 2014.

Nakamura, T**., T. Aono, T. Tsuda, A. G. Admiranto, E. Achmad, and Suranto,** Mesospheric gravity waves over a tropical convective region observed by OH airglow imaging in Indonesia, *Geophys. Res. Lett.*, 30(17), 1882, doi:10.1029/2003GL017619, 2003..

Nakamura, T. Higashikawa, A., and T. Tsuda, Seasonal variation of gravity waves observed with an OH CCD imager at Shigaraki (35°N,136°E), Japan, *Adv. Sp. Res.*, *24*(5), 561–564, doi:10.1016/S0273-1177(99)00201-X, 1999.

Pandya, R. E., and M. J. Alexander, Linear Stratospheric Gravity Waves above Convective Thermal Forcing, *J. Atmos. Sci.*, *56*(14), 2434–2446, doi:10.1175/1520-0469(1999)056<2434:LSGWAC>2.0.CO;2, 1999.

Paulino, I., Takahashi, H., Vadas, S.L., Wrasse, C.M., Sobral, J.H.A., Medeiros, A.F., Buriti, R. A., Gobbi, D., Forward ray-tracing for medium-scale gravity waves observed during the COPEX campaign, *J. Atmos. Solar-Terr. Phys.*, 90–91, 117-123, doi:10.1016/j.jastp.2012.08.006, 2012.

Piani, C., D. Durran, M. J. Alexander, and J. R. Holton, A Numerical Study of Three-Dimensional Gravity Waves Triggered by Deep Tropical Convection and Their Role in the Dynamics of the QBO, *J. Atmos. Sci.*, *57*(22), 3689–3702, doi:10.1175/1520-0469(2000)057<3689:ANSOTD>2.0.CO;2, 2000.

Picone, J.M., Hedin, A.E., Drob, D.P., Aikin, A.C.,NRLMSISE-00 empirical model of the atmosphere: statistical comparisons and scientific issues. *J. Geophys. Res*., 107, 1468 0148-0227, 2002.

Pragati, R.S., Parihar, N., Ghodpage, R., and Mukherjee, G.K., Characteristics of gravity waves in the upper mesospheric region observed by OH airglow, *Current Science* 98(3), 392-397, 2010.

Parihar, N., and Taori, A., An investigation of long-distance propagation of gravity waves under CAWSES India Phase II Programme, *Ann. Geophys.* 33, 547-560, 2015.

Pautet, P. D., M. J. Taylor, A. Z. Liu, and G. R. Swenson, Climatology of short-period gravity waves observed over northern Australia during the Darwin Area Wave Experiment (DAWEX) and their dominant source regions, *J. Geophys. Res. D Atmos.*, *110*(3), 1–13, doi:10.1029/2004JD004954, 2005.

Pramitha, M., M. Venkat Ratnam, A. Taori, B. V. Krishna Murthy, D. Pallamraju, and S. Vijaya Bhaskar Rao, Evidence for tropospheric wind shear excitation of high-phase-speed

gravity waves reaching the mesosphere using the ray-tracing technique, *Atmos. Chem. Phys.*, *15*(5), 2709–2721, doi:10.5194/acp-15-2709-2015, 2015.

Sivakandan, M., A. Taori, S. Sathishkumar, and A. Jayaraman, Multi-instrument investigation of a mesospheric gravity wave event absorbed into background, *J. Geophys. Res.*, doi:10.1002/2014JA020896, 2015.

Smith, A. K., Global Dynamics of the MLT, *Surv. Geophys.*, *33*(6), 1177–1230, doi:10.1007/s10712-012-9196-9,2012.

Suzuki, S., K. Shiokawa, Y. Otsuka, T. Ogawa, and P. Wilkinson, Statistical characteristics of gravity waves observed by an all-sky imager at Darwin, Australia, *J. Geophys. Res.*, 109, doi:10.1029/2003JD004336,2004.

Suzuki, S., Shiokawa, K., Hosokawa, K., Nakamura, K. and Hocking, W. K.: Statistical characteristics of polar cap mesospheric gravity waves observed by an all-sky airglow imager at Resolute Bay, Canada, *J. Geophys. Res. Sp. Phys.*, 114(1), 1–8, doi:10.1029/2008JA013652, 2009a.

Suzuki, S., Shiokawa, K., Liu, a. Z., Otsuka, Y., Ogawa, T. and Nakamura, T.: Characteristics of equatorial gravity waves derived from mesospheric airglow imaging observations, *Ann. Geophys.*, 27(4), 1625–1629, doi:10.5194/angeo-27-1625-2009, 2009b.

Taori, A., S. Raizada, M. V. Ratnam, C. A. Tepley, D. Nath, and A. Jayaraman, Role of Tropical Convective Cells in the Observed Middle Atmospheric Gravity Wave Properties from Two Distant Low Latitude Stations, *Earth Sci. Res.*, *1*(1), 87–97, doi:10.5539/esr.v1n1p87, 2012.

Taori, A., A. Jayaraman, and V. Kamalakar, Imaging of mesosphere-thermosphere airglow emissions over Gadanki (13.5°N, 79.2°E) - first results, *J. Atmos. Solar-Terrestrial Phys.*, *93*, 21–28, doi:10.1016/j.jastp.2012.11.007, 2013.

Taylor, M. J., and M. A. Hapgood, Identification of a thunderstorm as a source of short period gravity waves in the upper atmospheric nightglow emissions, *Planet. Space Sci.*, *36*(10), 975–985, doi:10.1016/0032-0633(88)90035-9, 1988.

Vadas, S.L., Fritts, D.C., Thermospheric responses to gravity waves: influences of increasing viscosity and thermal diffusivity. *J. Geophys. Res.*, 110, 15103, doi:10.1029/2004JD005574, 2005.

Vadas, S.L., Fritts, D.C., Reconstruction of the gravity wave field from convective plumes via ray tracing. *Ann. Geophys.*, 27, 147–177, 0992-7689, 2009.

Vadas, S.L., Liu, H.-l., Generation of large-scale gravity waves and neutral winds in the thermosphere from the dissipation of convectively generated gravity waves. *J. Geophys. Res.*, 114, A10310, doi:10.1029/2009JA014108, 2009.

Walterscheid, R. L., J. H. Hecht, R. A. Vincent, I. m. Reid, J. Woithe, and M. P. Hickey, Analysis and interpretation of airglow and radar observations of quasi-monochromatic gravity waves in the upper mesosphere and lower thermosphere over Adelaide, Australia (35°S, 138°E), *J. Atmos. Solar-Terrestrial Phys.*, *61*, 461–478, doi:10.1016/S1364-6826(99)00002-4, 1999.

Wrasse, C. M., Nakamura, T., Takahashi, H., Medeiros, A. F., Taylor, M. J., Gobbi, D., Denardini, C. M., Fechine, J., Buriti, R. A., Salatun, A., Suratno, Achmad, E. and Admiranto, A. G.: Mesospheric gravity waves observed near equatorial and low an middle latitude stations: wave characteristics and reverse ray tracing results, *Ann. Geophys.*, 24(12), 3229–3240, doi:10.5194/angeo-24-3229-2006, 2006.

Table 1. Predominnent wave propagation directions in different months.

Month and year	wave propagations in different direction				Total
	East (46-135)	South (136-225)	West (226-315)	North (316-45)	
Mar-12	Nil	2	2	10	14
Apr-12	2	Nil	1	4	7
Apr-13	1	Nil	Nil	4	5
Mar-14	1	2	1	5	9
Apr-14	3	2	Nil	10	15
Total	7	6	4	33	50

Table 2. Comparison of the present results with earlier small-scale wave measurements.

Station	Latitude, Longitude	Horizontal wavelength (km)	Phase speed (m/s)	Observed period (min.)	References
Shigaraki	35^{o}N,136^{o}E	5-60	0-100	0-30	Nakamura et al. (1999)
Rikubetsu	43.5^{o}N,143.8^{o}E	10-42 (OH) 10-58 ($O^{1}S$)	~0-100 ~10-110		Ejiri et al., (2003)
Cachoeira Paulista	23^{o}S,45^{o}W	5-60	10-80	6-34	Medeiros et al., (2003)
Tanjungsari	6.9^{o}S,107.9^{o}E	3-80	10-95	5-13	Nakamura et al., (2003)
Darwin	12.4^{o}S,131^{o}E	20-90	0-90		Suzuki et al., (2004)
Buckland Park	34.5^{o}S,138.5^{o}E	20-200	20-250	40-240	Ding et al., (2004)
Cariri	7.4^{o}S, 36.5^{o}W	~5-40	1-90	~5-30	Medeiros et al., (2007); Wrasse et al., (2006)
Resolute Bay,	74.7^{o}N,265.1^{o}E	~10-70	10-110		Suzuki et al., (2009a)
Kototabang	0.2^{o}S, 100.3^{o} E	25-95	5-125		Suzuki et al., (2009b)
Mt. Bohyun, Korea	36.2^{o}N,128.9^{o} E	10-45	0-80	5-45	Kim et al. (2010)
Xinglong	40.2^{o}N,117.4^{o} E	~10-55	10-100	2-20	Li et al., (2011a)
Maui	20.7^{o}N,156.3^{o}W	~10-120	~0-150	~5-30	Li et al., (2011b)
Syowa Station	69^{o}S,0-40^{o}E	10-60	0-150	3-65	Matsuda et al., (2014)
Tirunelveli	8.7^{o}N, 77.8^{o}E	5-45	10-140	3-20	Lakshmi Narayanan and Gurubaran, (2013)
Gadanki	13.5^{o}N, 79.2^{o}E	12-**42**	20-90	4-20	**Present Study**

Figure Captions:

Figure 1. A sample figure depicting the gravity wave signatures. One may see the propagation of features. The green color box show the dominant wave fronts, while the yellow arrows reveal their propagation direction at an angle Ɵ.

Figure 2. The distribution of horizontal wavelengths of the observed waves in March-April 2012 and 2014 and April 2013.

Figure 3. The distribution of the observed phase velocity of waves in March-April 2012 and 2014 and April 2013.

Figure 4. The distribution of observed periods of the in March-April 2012 and 2014 and April 2013.

Figure 5. left side (figure 5a) depicting the observed phase speed and direction of horizontal propagation of gravity waves and right side plots depicting the reverse ray tracing results in (b) zero wind (top side) as well as in (c) HWM-07 model wind (bottom side) condition in March-April 2012 and 2014 and April 2013. The red color arrows (lines) indicate March events while blue arrows (lines) show the events noted in April month. In polar plot 0^o belongs to the North and the inner dotted circles indicate the horizontal phase speed of the observed wave at an interval of 20 m/s. In right side plots red (blue) dots indicate the ray termination point in March (April).

Figure 6. Same as figure 5 but only for the year 2012.

Figure 7. The average of daily mean OLR for the days when waves were observed in airglow image data in March and April 2012. The location of measurement is shown as **asterisk** in each map.

Figure 8. The daily mean OLR data and ray paths for different wave event noted in 27 March 2012. Ray tracing plots blue (red) color line indicates ray paths in model wind (zero wind) condition and the blue color triangle show observation location (Gadanki). Plus and filled square symbols indicate where the gravity waves have the maximum amplitude into the thermophere. Star and open square show where/when the gravity waves have less than 1% of their initial amplitude. From the OLR plot one may note the occurence of convective events at northern Indian locations.

Figure 9. Same as figure 5 but for the year 2013.

Figure 10. Same as figure 7 but for the year 2013.

Figure 11. Same as figure 5 but for the year 2014.

Figure 12. Same as figure 7 but for the year 2014.

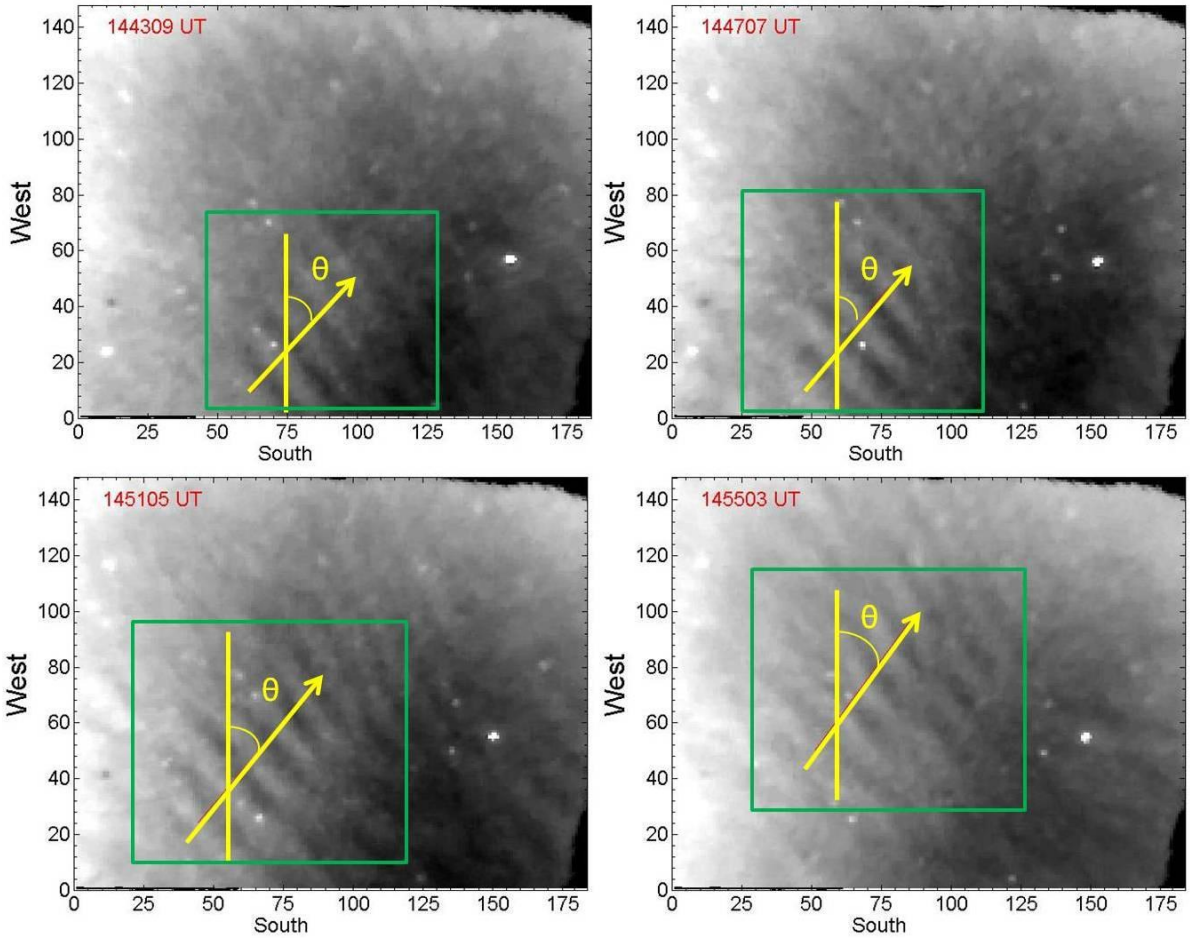

Figure 1. A sample figure depicting the gravity wave signatures. One may see the propagation of features. The green color box show the dominant wave fronts, while the yellow arrows reveal their propagation direction at an angle Θ.

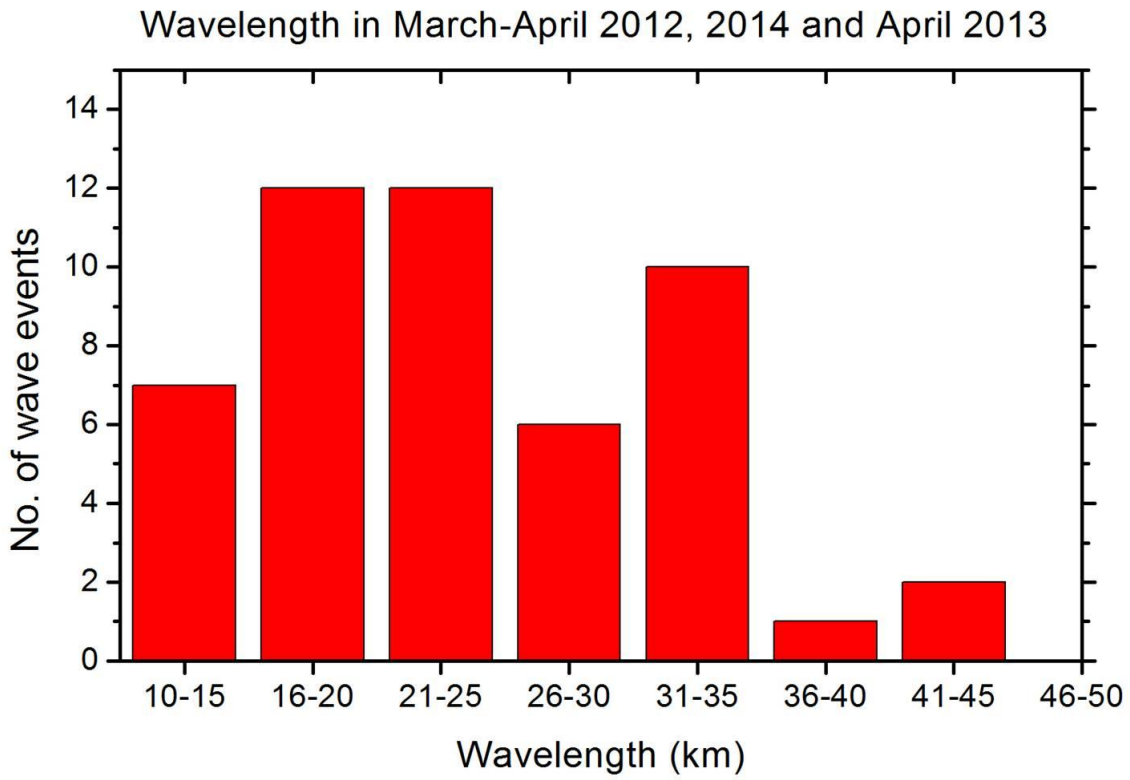

Figure 2. The distribution of horizontal wavelengths of the observed waves in March-April 2012 and 2014 and April 2013.

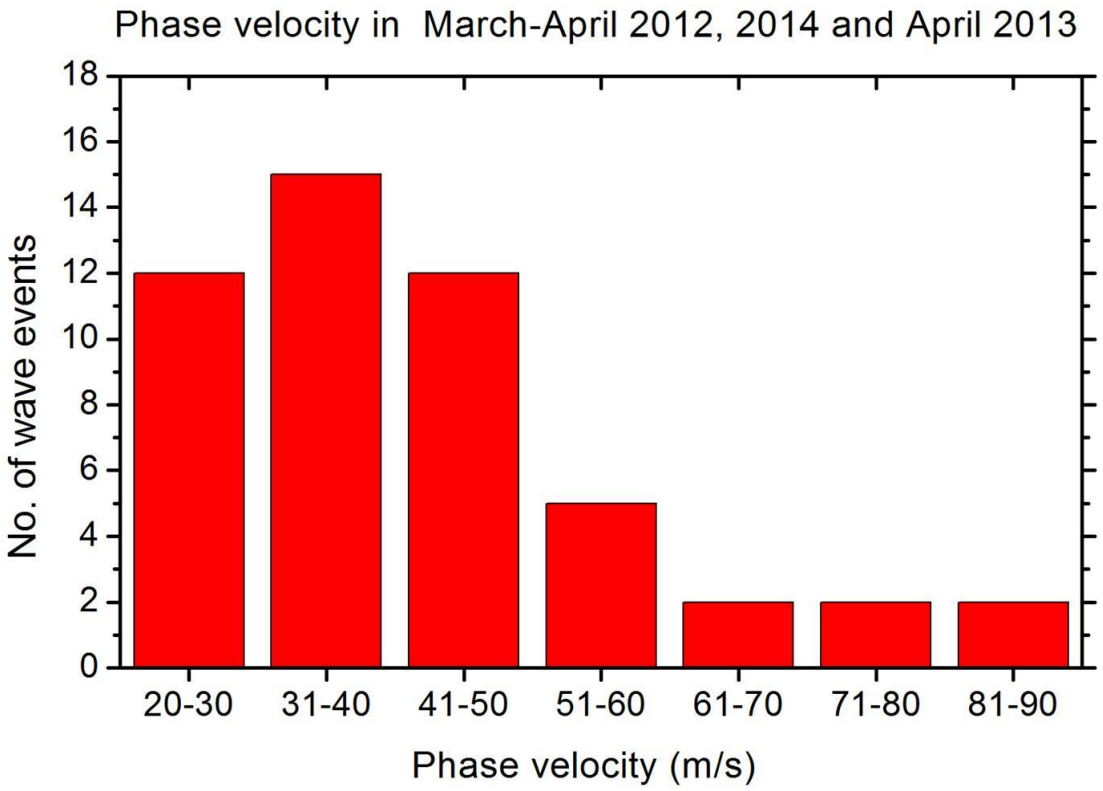

Figure 3. The distribution of the observed phase velocity of waves in March-April 2012 and 2014 and April 2013.

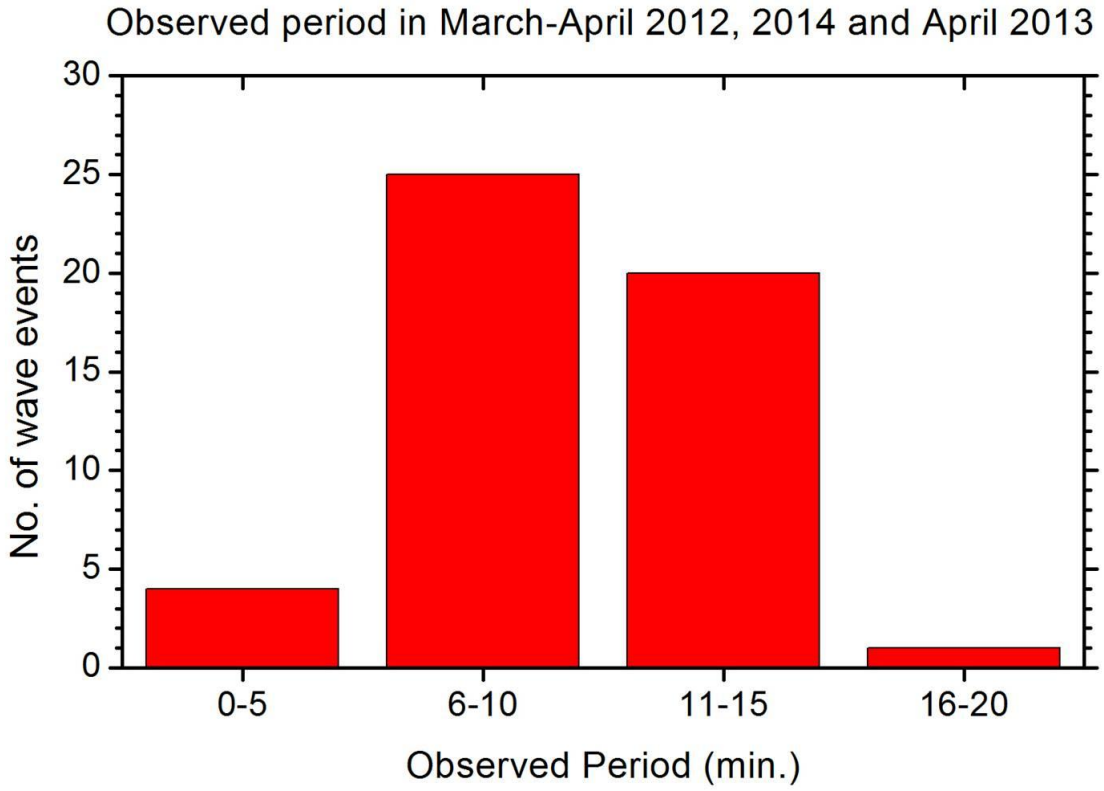

Figure 4. The distribution of observed periods of the in March-April 2012 and 2014 and April 2013.

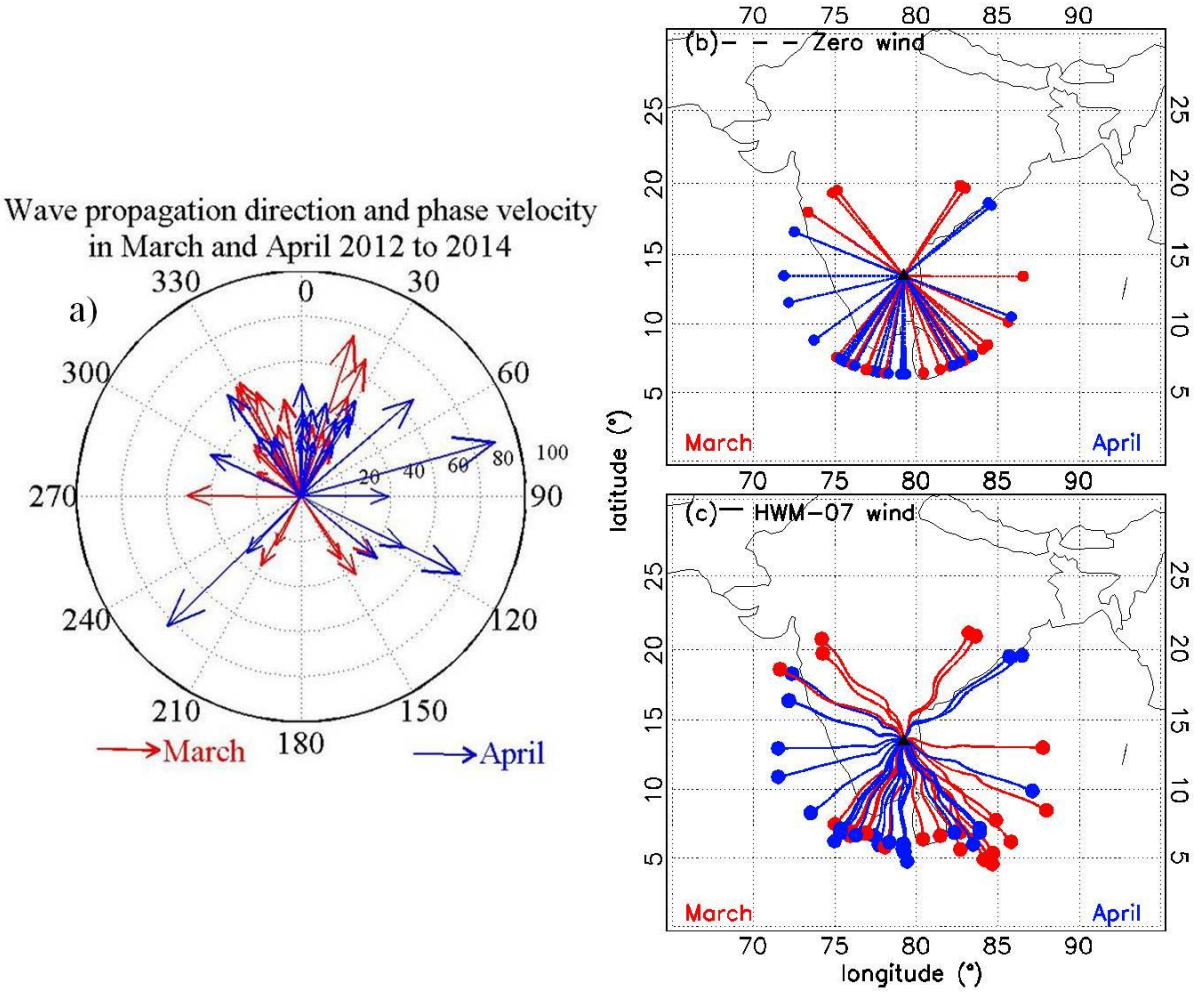

Figure 5. left side (figure 5a) depicting the observed phase speed and direction of horizontal propagation of gravity waves and right side plots depicting the reverse ray tracing results in (b) zero wind (top side) as well as in (c) HWM-07 model wind (bottom side) condition in March-April 2012 and 2014 and April 2013. The red color arrows (lines) indicate March events while blue arrows (lines) show the events noted in April month. In polar plot 0^{o} belongs to the North and the inner dotted circles indicate the horizontal phase speed of the observed wave at an interval of 20 m/s. In right side plots red (blue) dots indicate the ray termination point in March (April).

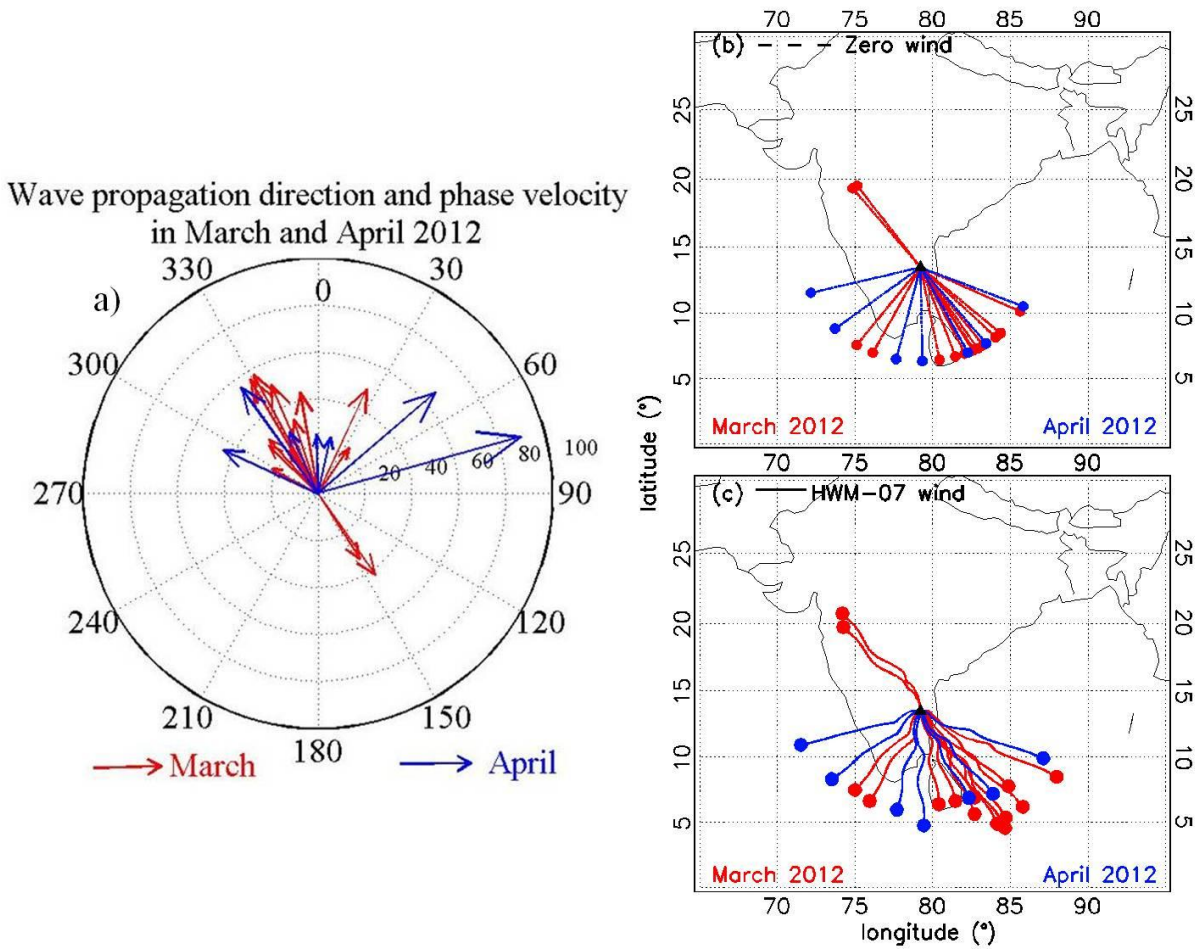

Figure 6. Same as figure 5 but only for the year 2012.

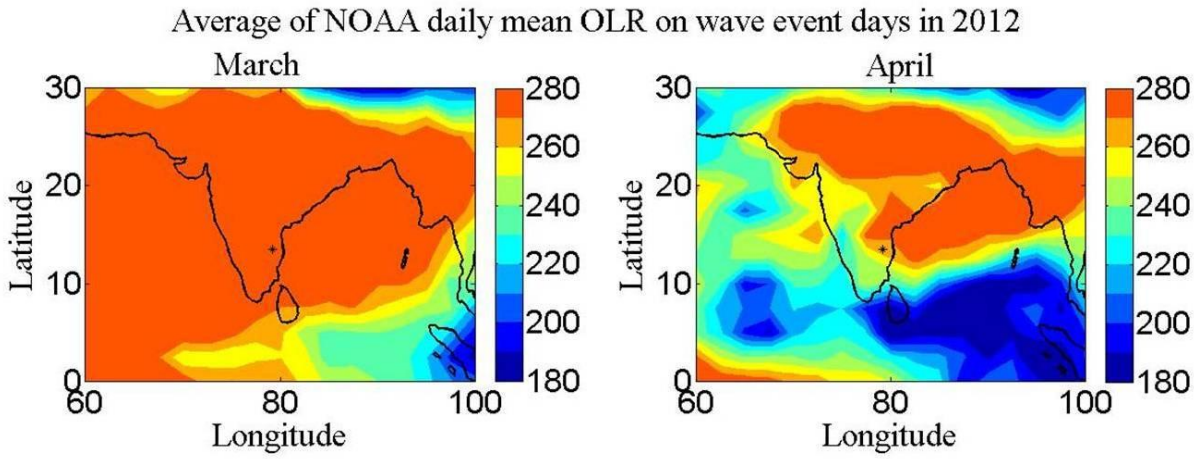

Figure 7. The average of daily mean OLR for the days when waves were observed in airglow image data in March and April 2012. The location of measurement is shown as asterisk in each map.

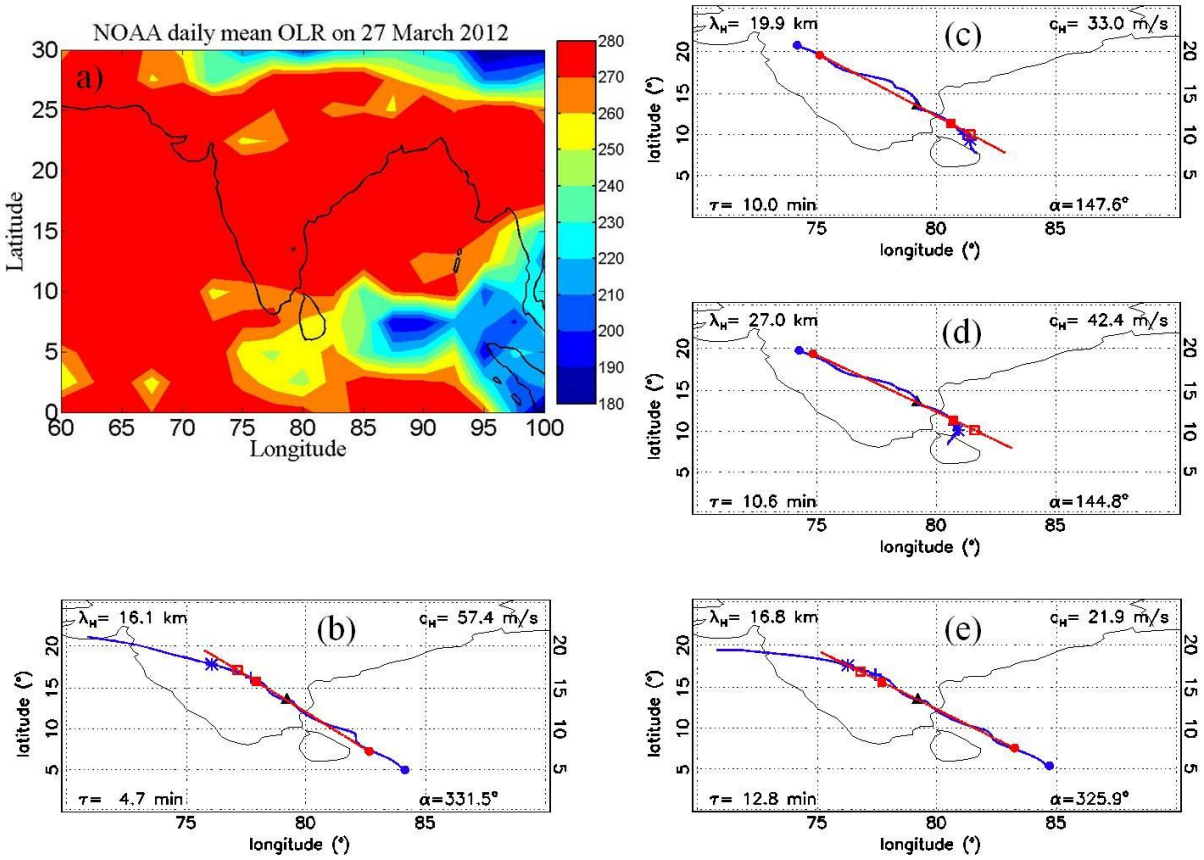

Figure 8. The daily mean OLR data and ray paths for different wave event noted in 27 March 2012. Ray tracing plots blue (red) color line indicates ray paths in model wind (zero wind) condition and the blue color triangle show observation location (Gadanki). Plus and filled square symbols indicate where the gravity waves have the maximum amplitude into the thermophere. Star and open square show where/when the gravity waves have less than 1% of their initial amplitude. From the OLR plot one may note the occurence of convective events at northern Indian locations.

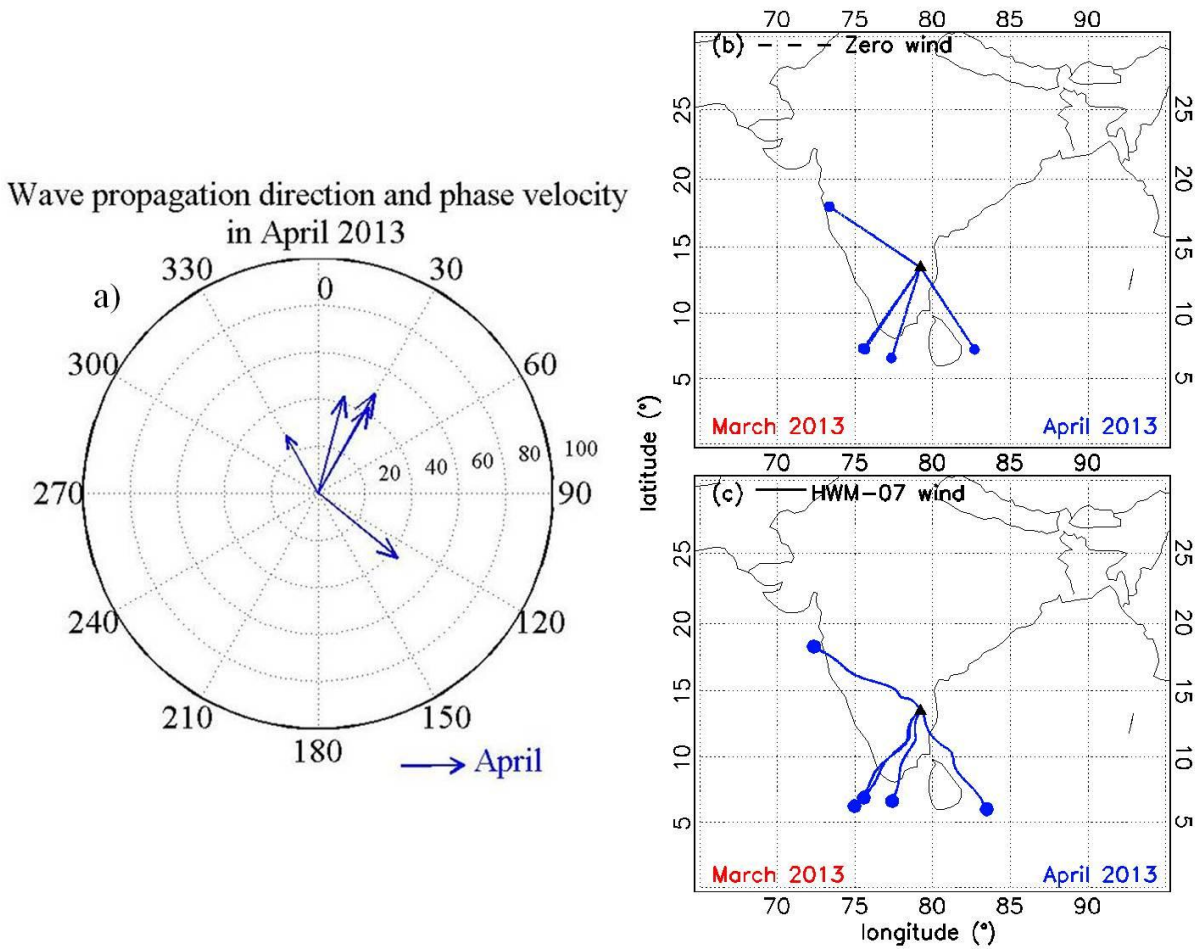

Figure 9. Same as figure 5 but for the year 2013.

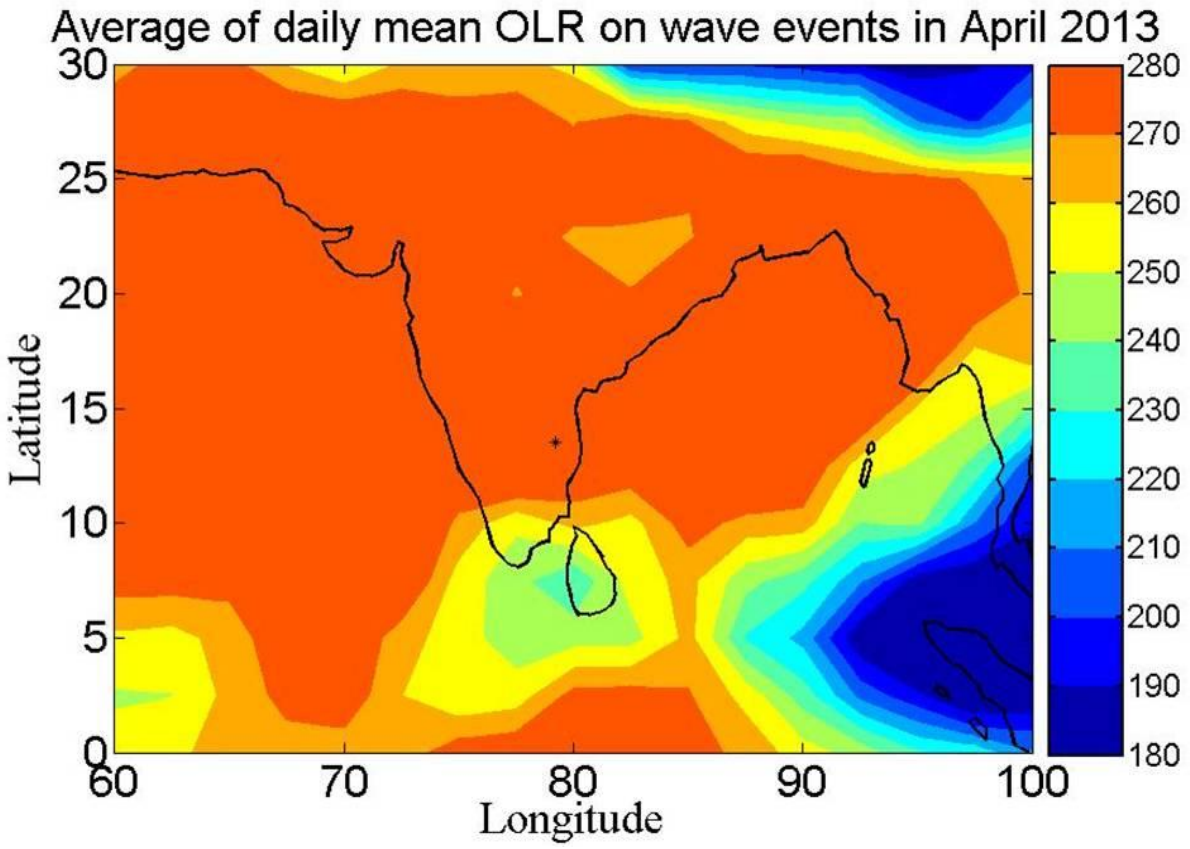

Figure 10. Same as figure 7 but for the year 2013.

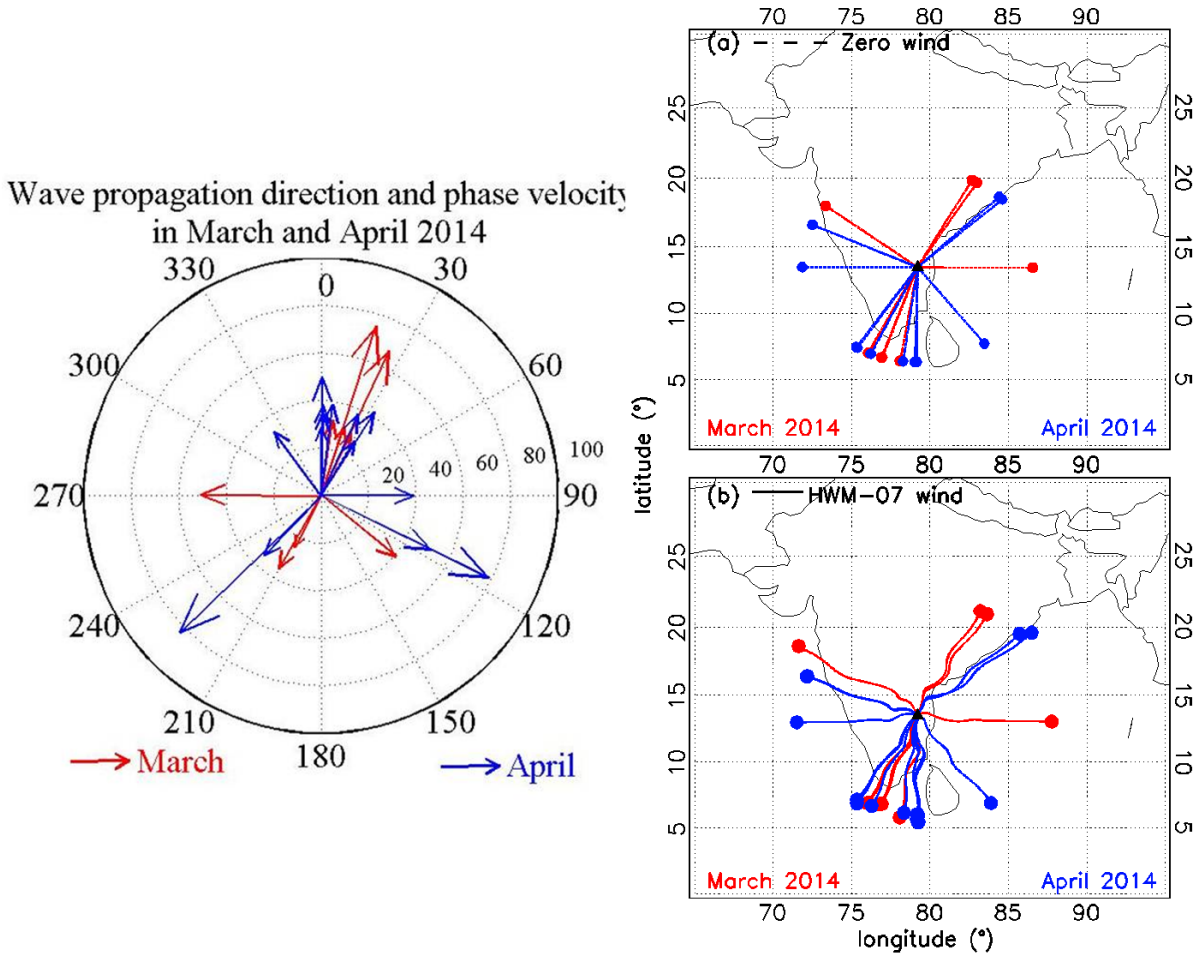

Figure 11. Same as figure 5 but for the year 2014.

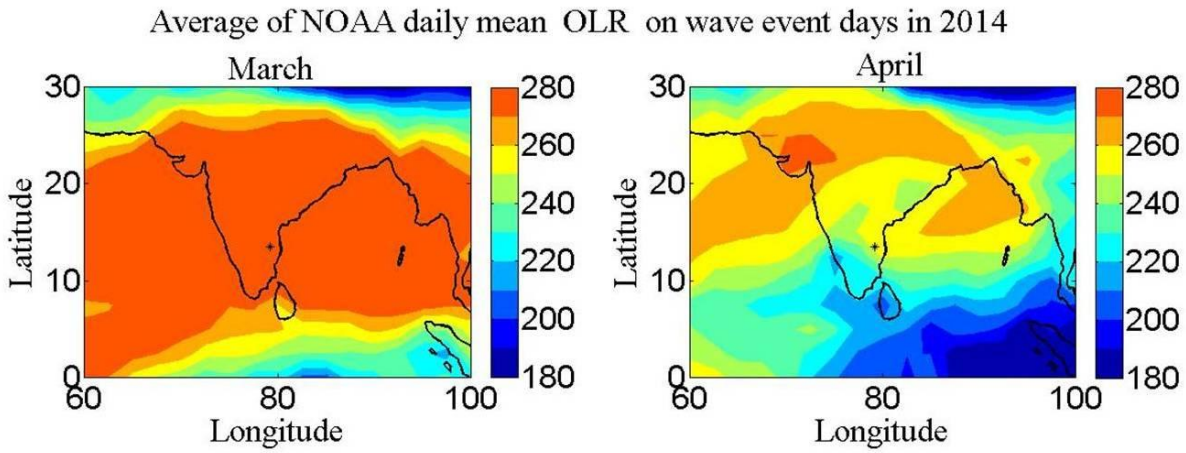

Figure 12. Same as figure 7 but for the year 2014.